INTERNATIONAL JOURNAL OF
RADIATION ONCOLOGY • BIOLOGY • PHYSICS
www.redjournal.org

BIOLOGY CONTRIBUTION

Acute Hypoxia Does Not Alter Tumor Sensitivity to FLASH Radiation Therapy

Ron J. Leavitt, PhD,[*] Aymeric Almeida, MSc,[*] Veljko Grilj, PhD,[†] Pierre Montay-Gruel, PhD,[*,‡,§] Céline Godfroid, MSc,[*] Benoit Petit,[*] Claude Bailat, PhD,[†] Charles L. Limoli, PhD,[‖] and Marie-Catherine Vozenin, PhD[*]

[*]*Radiation Oncology Laboratory, Department of Radiation Oncology, Lausanne, University Hospital and University of Lausanne, Lausanne, Switzerland;* [†]*Institute of Radiation Physics, University Hospital and University of Lausanne, Lausanne, Switzerland;* [‡]*Radiation Oncology Department, Iridium Netwerk, Wilrijk (Antwerp), Belgium;* [§]*Antwerp Research in Radiation Oncology (AReRO), Center for Oncological Research (CORE), University of Antwerp, Antwerp, Belgium; and* [‖]*Department of Radiation Oncology, University of California, Irvine, California*

Received Oct 7, 2023; Accepted for publication Feb 8, 2024

Purpose: Tumor hypoxia is a major cause of treatment resistance, especially to radiation therapy at conventional dose rate (CONV), and we wanted to assess whether hypoxia does alter tumor sensitivity to FLASH.

Methods and Materials: We engrafted several tumor types (glioblastoma [GBM], head and neck cancer, and lung adenocarcinoma) subcutaneously in mice to provide a reliable and rigorous way to modulate oxygen supply via vascular clamping or carbogen breathing. We irradiated tumors using a single 20-Gy fraction at either CONV or FLASH, measured oxygen tension, monitored tumor growth, and sampled tumors for bulk RNAseq and pimonidazole analysis. Next, we inhibited glycolysis with trametinib in GBM tumors to enhance FLASH efficacy.

Results: Using various subcutaneous tumor models, and in contrast to CONV, FLASH retained antitumor efficacy under acute hypoxia. These findings show that in addition to normal tissue sparing, FLASH could overcome hypoxia-mediated tumor resistance. Follow-up molecular analysis using RNAseq profiling uncovered a FLASH-specific profile in human GBM that involved cell-cycle arrest, decreased ribosomal biogenesis, and a switch from oxidative phosphorylation to glycolysis. Glycolysis inhibition by trametinib enhanced FLASH efficacy in both normal and clamped conditions.

Conclusions: These data provide new and specific insights showing the efficacy of FLASH in a radiation-resistant context, proving an additional benefit of FLASH over CONV.

Corresponding author: Marie-Catherine Vozenin, PhD; E-mail: marie-catherine.vozenin@hcuge.ch

Marie-Catherine Vozenin's current location is Radiotherapy and Radiobiology Sector, Radiation Therapy Service, University Hospital of Geneva, Geneva, Switzerland.

Disclosures: Funding was provided by Swiss National Science Foundation grant MAGIC - FNS CRS II5_186369 (to M.C.V. and supporting R.J. L., V.G.), National Institutes of Health grant P01CA244091-01 (to M.C.V. and C.L.L. and supporting A.A., V.G.), and Swiss National Science Foundation grant FNS N 31003A_156892 (supporting P.M.G.). The authors declare no competing financial interests.

Data Sharing Statement: Research data have been deposited in NCBI's Gene Expression Omnibus and are accessible through GEO Series accession number GSE223607 (https://www.ncbi.nlm.nih.gov/geo/query/acc.cgi?acc=GSE223607). All data and code are available upon request.

Acknowledgments—We thank Prs J. Bourhis and F. Bochud for their support, Dr S. Vinogradov for expert technical advice, Dr T. Boehlen for help in formatting figures, J. Ollivier for technical help, and K. Sprengers for help in radiation experiments. We also thank the Lausanne Genomic Technologies Facility and the animal facility at Epalinges.

Supplementary material associated with this article can be found in the online version at doi:10.1016/j.ijrobp.2024.02.015.

https://doi.org/10.1016/j.ijrobp.2024.02.015

Introduction

Tumor hypoxia is a primary factor of resistance to radiation therapy (RT) and chemotherapy (CT) treatments. Reduced oxygen tension is very common in solid tumors,[1] as it develops in response to a dense and metabolically active tumor-cell population associated with poor, uneven, and morphologically abnormal vasculature resulting in acute (proximal to host blood vessel) or chronic (distal to any vasculature) hypoxia. Although the lack of oxygen itself is the primary cause of radioresistance, irregularities in the vascular network are mainly responsible for CT resistance preventing drug access to the tumor. At the cellular level, hypoxia causes rapid activation of hypoxia-inducible factor (HIF) transcription factors[2] as acute survival mechanisms. HIFs transactivate an array of genes involved in angiogenesis, pH balance, cell apoptosis, and a shift to anaerobic metabolism essential for tumor survival and resistance to treatment. Multiple attempts to overcome tumor hypoxia have been proposed including hypoxia-activated prodrugs, hyperbaric oxygen breathing, 60% supplemental oxygen, allosteric hemoglobin modifiers, molecules that improve oxygen diffusion, and oxygen transport agents (hemoglobin-based or fluorocarbon-based).[3] Most of these strategies have led to negative results on tumor control and enhanced normal tissue toxicity. To date, no effective anticancer therapy against hypoxic tumors is available.

Previously, a novel RT approach called FLASH was developed based on ultrahigh-dose-rate irradiation.[4,5] The main interest of FLASH is its capacity to enhance the therapeutic window by sparing normal tissue from radiation-induced toxicities while eliciting the same tumor kill compared with isodoses of conventional dose-rate RT, a biologic effect that has been called the "FLASH effect." Although currently the availability of FLASH-capable clinical beams remains the main obstacle for the clinical translation of FLASH,[4] understanding its differential effect at the normal tissue versus tumor level remains an important goal to further decipher the mechanisms of the FLASH effect[6] and facilitate clinical translation.

Nearly every preclinical cancer model tested has shown identical tumor response when FLASH and the conventional dose rate (CONV) were compared.[7-12] Importantly, to date, there has not been any investigation performed to evaluate the efficacy of FLASH on extremely hypoxic, radioresistant tumors.

To rectify this critical gap in knowledge, we focused the present work on studying the effect of intratumoral oxygen tension on tumor response to FLASH versus CONV. Here we implemented subcutaneous tumors and modulated intratumoral oxygen tension by vascular clamping or carbogen breathing. Our results show that, contrary to CONV, FLASH maintains its antitumor efficacy ***under clamped conditions***. We performed subsequent molecular analysis using RNAseq profiling at acute and relapse time points. At 24 hours after RT, expression data pointed toward specific inhibition of proliferation and translation-associated genes as well as metabolic shifts after FLASH *versus* CONV. Specifically, we identified glycolysis as a possible escape/survival pathway after exposure to FLASH and inhibited it using trametinib in an attempt to amplify tumor response.

Methods and Materials

Animal experiments

Female Swiss Nude mice (NU(Ico)-*Foxn1*^{nu}; Charles River, strain code: 620) were purchased for subcutaneous tumor experiments using the U-87 MG, SV2, and mEERL95 tumor models. Experiments were duplicated with SV2 and mEERL95 tumor models in female C57BL/6J (Charles River, strain code: 632) and C57BL/6JRj (Janvier Labs) mice, respectively. Animal experiments were approved by the Swiss Ethics Committee for Animal Experimentation (VD 3241 − VD 3603 − VD 3670 − VD 3797) and performed within institutional guidelines.

Cell culture and *in vivo* tumor model

U-87 MG (HTB-14, ATCC) human glioblastoma (GBM) cells were cultured under standard conditions (37 °C, 5% CO_2) in complete medium containing Dulbecco's Modified Eagle Medium + GlutaMAX (4.5 g/L D-Glucose, Pyruvate; 31966-021; Thermo Fisher Scientific) and supplemented with 10% fetal bovine serum (F7524; Sigma-Aldrich). The U-87 MG subcutaneous human GBM model consists of injecting 10^7 U-87 MG human GBM cells in 100 μL of phosphate-buffered saline (PBS) in the right flank of female Swiss Nude mice. For SV2 and mERRL95, cell culture and *in vivo* tumor models are described in Appendix E1.

Irradiation device, procedure, and follow-up

Irradiations were performed using a prototype 6 MeV electron beam linear accelerator of type Oriatron 6e (eRT6; PMB Alcen), available at Lausanne University Hospital and described previously.[13] Dosimetry has been extensively described and published to ensure reproducible and reliable biologic studies. All FLASH irradiations were performed at a mean dose rate greater than or equal to 100 Gy/s and at an intrapulse dose rate greater than 5.6×10^6 Gy/s (Table E1).

Irradiations were performed when tumor volume reached a mean between 60 and 80 mm^3. Mice were randomly assigned to 1 of 3 different irradiation groups (NIR [nonirradiated], CONV, and FLASH) and to 1 of 3 different oxic-condition groups (normal, clamped, and carbogen). Initial mean tumor volumes were similar in all groups (NIR normal: 66.2 ± 6.1 mm^3, NIR clamped: 57.8 ± 9.5 mm^3, NIR carbogen: 59.8 ± 10.5 mm^3, CONV normal: 63.8 ± 6.2 mm^3, CONV clamped: 73.2 ± 6.1 mm^3, CONV carbogen:

63.1 ± 5.2 mm^3, FLASH normal: 63.3 ± 5.0 mm^3, FLASH clamped: 71.1 ± 4.6 mm^3, and FLASH carbogen: 61.4 ± 4.4 mm^3).

Tumors were irradiated by positioning the tumor-bearing part of the skin in extension behind and in contact with the opening of the 1.7-cm diameter graphite applicator, to limit the dose to the intestines. A 5-mm solid water plate was placed behind the skin to ensure homogenous dose delivery. For irradiations under carbogen conditions, mice were anesthetized with isoflurane and carbogen (95% O_2, 5% CO_2) for at least 20 minutes, including the irradiation time. For irradiations in clamped conditions, tumors were clamped with a vascular clamp at least 15 minutes before and during the irradiation. All tumors were treated with a single dose of 20 Gy. For all regimens, FLASH and CONV irradiation modalities were compared.

Tumor volume was measured 3 times per week by the same researcher (for the duration of each independent experiment) using a digital caliper and calculated using the formula for an oblate ellipsoid: $\frac{width^2 \times length}{2}$. Relative tumor volumes were calculated by percentage of volume at the time of irradiation $\left(\frac{Current\ volume}{Volume\ at\ T_0} \times 100\%\right)$.

Intratumoral oxygen tension measurements using the OxyLED system and Oxyphor PtG4 probe

On the day of the experiment, animals were anesthetized as described in Appendix E1. Once anesthetized, 25 μL of Oxyphor PtG4 probe (200 μM; Oxygen Enterprises Ltd) was injected intravenously. After 30 minutes to ensure the spread and accumulation of the probe, the OxyLED excitation laser and optical fiber (Oxygen Enterprises Ltd) was placed a few millimeters away from the tumor to perform the measurement of the intratumoral oxygen tension. All measurements were performed with the animals under anesthesia. Measurements were taken for all 3 oxygenation conditions (n = 3 per condition).

Validation of the different oxygen conditions with pimonidazole

To confirm the different oxygenation conditions in the tumor groups, mice from each oxic-condition group (n = 4 per group) were injected intravenously with 60 mg/kg body weight of pimonidazole (HP1-100Kit; Hypoxyprobe), 90 minutes before tumor sampling. For normal conditions, injection was followed by 90 minutes of normal air breathing. For carbogen conditions, injection was followed by 90 minutes of carbogen breathing. For clamped conditions, injection was followed by 15 minutes of air breathing followed by 7 minutes of tumor clamping and finally 68 minutes of air breathing.

Tumors were then collected, fixed in FineFIX (84-1717-00; Biosystems), embedded in paraffin, and finally cut into 4-μm sections. Tumor hypoxia was validated on tumor sections using mouse antipimonidazole monoclonal antibody (1:50; HP1-100Kit; Hypoxyprobe) incubated for 1 hour at room temperature. The sections were then incubated for 1 hour with a donkey antimouse AF488 secondary antibody (1:250; A21202, Life Technologies). Image acquisition was performed using an upright Zeiss Axiovision microscope.

Sampling and high-throughput sequencing

For the RNAseq study, mice (n = 3-6 for each group) were irradiated in the same conditions and with the same dose as described previously. Tumors were sampled 24 hours after RT or 7 days after the start of tumor regrowth (NIR: 35 days; CONV clamped: 40 days; CONV normal: 41 days; CONV carbogen: 44.4 ± 0.6 days, FLASH clamped: 41 days, FLASH normal: 41 days, FLASH carbogen: 43.0 ± 1.2 days). RNA extraction, library preparation, and sequencing were performed as detailed in Appendix E1.

Bioinformatic analysis

Raw FASTQ files were uploaded to the European Galaxy server (www.usegalaxy.eu) for further manipulation and processing. Read quality was assessed using FastQC. Read trimming was not necessary[14]; thus, alignment was immediately performed. The RNA STAR aligner (version 2.7.8a[15]) was used to align the reads to the human genome (hg38, for the human tumor cells) and the mouse genome (mm10, for the mouse vasculature within the tumor sample), with NM-tag turned on for subsequent XenofilteR analysis. Binary alignment (BAM) files from all sequencing lanes for each sample were merged at this point (within alignments to the same species) using the Samtools merge tool (version 1.13[16]). These merged and paired alignments for each sample were used as input for XenofilteR (version 1.6[17]) for filtering of mouse reads from the human alignment, which was implemented in R (version 4.1.0[18]) using the RStudio environment (version 1.4.1717[19]). These filtered reads were then counted for annotated genes using featureCounts (version 2.0.1[20]) in Galaxy. Raw counts tables were imported back into RStudio for differential gene expression and pathway analyses using the DESeq2 (version 1.34.0[21]) and clusterProfiler (version 4.2.0[22]) packages. Plots were generated using the ggplots2 (version 3.3.5[23]), pheatmap (version 1.0.12[24]), and Pathview (version 1.32.0[25]) packages.

Adjuvant trametinib and vehicle treatments

Trametinib (C3822, ALSACHIM) was dissolved in dimethyl sulfoxide (D4540; Sigma-Aldrich) to a concentration of 10 mM (~6.15 mg/mL) and kept in aliquots at −80°C until use. On treatment day, an aliquot of working solution was thawed and added to sterile PBS for gavage. dimethyl sulfoxide was added to PBS for the vehicle treatment. Trametinib

was administered daily over the course of 2 weeks (days 1-15 post-RT) at a concentration of 1 mg/kg body weight by oral gavage in 200 μL of total volume.

Statistical analysis

Statistical analyses were carried out using GraphPad Prism (v9.1) software. For the tumor growth curve data, *P* values comparing tumor growth delay curves were derived from an endpoint test using a 1-way analysis of variance (ANOVA; if Gaussian distribution) or Kruskal-Wallis (if non-Gaussian distribution) test with *post hoc* Šídák or Dunn's correction for multiple testing, respectively. Tumor doubling times were calculated by natural-log-transformation of relative tumor volumes, followed by line fitting (only log-linear range), followed by calculation of the day value where the fitted line crosses the doubling threshold. When standard deviations were consistent among groups, *P* values for group comparisons of doubling time were derived from a normal one-way ANOVA test with *post hoc* Šídák correction for multiple testing. When standard deviations were not consistent among groups, *P* values for group comparisons of doubling time were derived from a Brown-Forsythe and Welch one-way ANOVA test with *post hoc* Dunnett T3 correction for multiple testing. *P* values comparing survival curves were derived from the log rank (Mantel-Cox) test. For RNAseq analysis, all adjusted *P* values had false discovery rate correction applied using the Benjamini-Hochberg procedure.[26] Results were expressed as mean values ± SEM in figures, mean values ± SEM in the text, and all analyses considered a value of $P < .05$ to be statistically significant unless specified otherwise.

Results

Acute hypoxia induces resistance to CONV but not FLASH in various experimental subcutaneous tumors

We used a human GBM (U-87 MG) xenograft model implanted subcutaneously and modulated the tumor oxygen tension using a vascular clamp or carbogen breathing. Results showed that tumor growth delay and survival rate were retained when clamped tumor were irradiated with 20 Gy FLASH (Fig. 1A, B). The mean doubling time of U-87 tumors was 19.1 ± 1.0 days when NIR and unmodified in oxygen tension (Fig. 1C). After CONV, the mean doubling time of the tumor was 34.5 ± 1.5 days in normal, 25.4 ± 1.0 days in clamped, and 42.2 ± 1.4 days in carbogen. After FLASH, the mean doubling time of the tumor was 31.2 ± 0.8 days in normal, 30.7 ± 1.3 in clamped, and 43.0 ± 2.5 days in carbogen. There was no significant difference between CONV and FLASH mean doubling times in normal (adjusted $P = .353$) or carbogen conditions (adjusted $P > .999$), whereas in clamped conditions, FLASH remained efficacious to delay tumor growth ($P = .999$ vs FLASH normal and $P = .025$ vs CONV clamped). To confirm the oxygenation conditions, we measured intratumoral oxygen tension before treatment via real-time oxygen readings using the OxyLED detector and Oxyphor PtG4 probe (Oxygen Enterprises Ltd; Figs. 1D and E1) and hypoxia (in the clamped condition) was confirmed posttreatment using pimonidazole staining (Fig. 1E).

We were able to replicate the enhanced efficacy of FLASH compared with CONV in clamped tumors multiple times by different experimenters using the same U-87 GBM model (Fig. E2). Additionally, we obtained similar results using SV2 mouse lung cancer and mEERL95 mouse head and neck cancer cell lines engrafted into Swiss Nude mice and immunocompetent C57BL/6J or C57BL/6JRj mice (Figs. E3 and E4), indicating a minimal contribution of the adaptive immune system to the antitumor effect of FLASH in hypoxic tumors. These data show a superior efficacy of FLASH in hypoxic tumors compared with CONV.

Existence of a FLASH-specific genomic imprint

To determine the mechanism of the antitumor efficacy triggered by FLASH versus CONV, we performed bulk RNAseq studies at early (24 hours post-RT) and more protracted (1-week post-tumor-recurrence) time points. The analysis included only the tumor component, as subcutaneously grown tumor nodules are mainly composed of tumor cells. Additionally, after alignment, we applied a deconvolution step to discriminate between human component (tumor) and mouse tissue contamination (host). Overall, we observed more top-level transcriptional differences in the 24-hour time point (Fig. E5A, principal component [PC] 1 accounting for 78% of variance). As shown on the heatmap (Fig. E5B), FLASH samples (green) tended to cluster further away from NIR samples (blue) compared with CONV samples (red). For the samples taken at the later time point post-RT, PCA (principal components analysis; Fig. E5C, PC1 accounting for 39% of variance) revealed a good clustering of the NIR groups (circle, left), whereas all the RT-treated tumors clustered together without distinction based on RT modality or oxygenation condition. We confirmed this pattern with the heatmap (Fig. E5D), suggesting that at this late time point, the genomic imprint is related to recurrence.

FLASH efficacy in hypoxic conditions is associated with a specific genomic imprint

Focusing on the normal and clamped conditions 24 hours post-RT, the PCA and heatmap showed that treatment modalities and tumor oxygen tensions associated with the longest tumor growth delay (CONV normal, FLASH normal, and FLASH clamped) are clustering together (Fig. 2A, B).

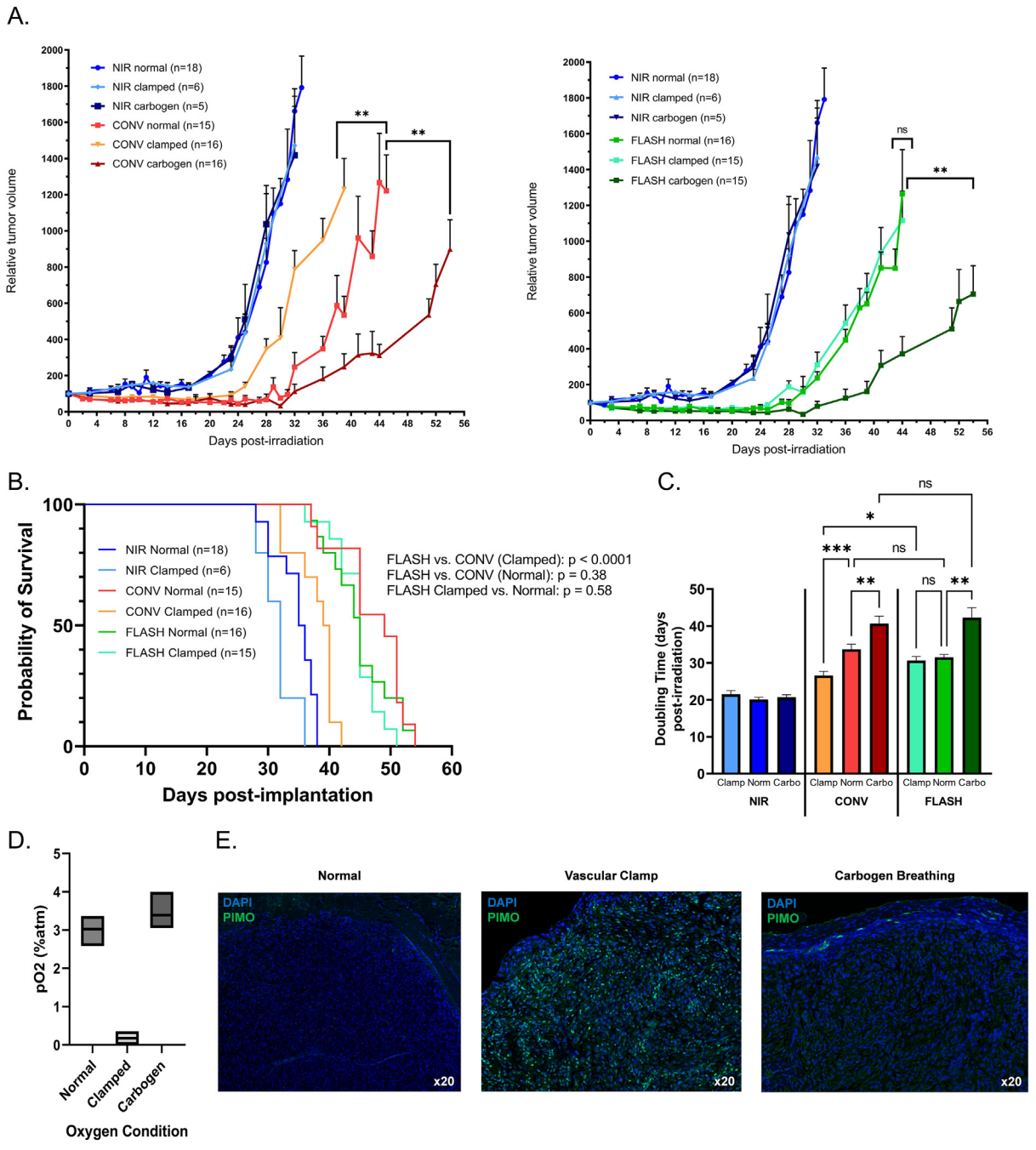

Fig. 1. FLASH, unlike CONV, maintains equivalent tumor control even in acutely hypoxic tumors. (A) Relative tumor volume of U-87 MG implanted subcutaneously in the flank of female nude mice treated with a 20-Gy single fraction delivered with CONV (left) or FLASH (right) with different oxygenation conditions (normal, clamped, carbogen). Nonirradiated (NIR) controls shown for each condition. Mean relative tumor volume ± SEM, N = 5 to 18 animals per group, as indicated for each group. *P* values (CONV) derived from endpoint analysis (minimum 4 measurements/group) using a Kruskal-Wallis test with *post hoc* Dunn's correction for multiple testing. *P* values (FLASH) derived from endpoint analysis using a one-way ANOVA test with *post hoc* Šídák correction for multiple testing: $^{**}P < .01$. (B) Kaplan-Meier survival curves for animals stratified by radiation modality and tumor oxygenation. *P* values derived from log rank (Mantel-Cox) test. (C) Doubling times calculated for each group. Mean days post-RT ± SEM, N = 5 to 18 animals per group. *P* values derived from Brown-Forsythe and Welch ANOVA with *post hoc* Dunnett T3 correction for multiple testing: $^{*}P < .05$; $^{**}P < .01$; $^{***}P < .001$. (D) Measured levels of oxygen from subcutaneous U-87 MG tumors *in vivo* taken using Oxyphor PtG4 (Oxygen Enterprises Ltd) phosphorescent probe with platinum core injected intravenously and detected using the OxyLED laser attachment and detector. Boxes minimum to maximum; median line drawn. (E) Pimonidazole immunostaining on tumor sections after manipulating oxygenation conditions: normal, vascular clamp, or carbogen breathing—each without RT. Green, pimonidazole (PIMO); blue, DAPI. *Abbreviations:* CONV = conventional dose rate; DAPI = (4′,6-diamidino-2-phenylindole); ns = not significant; RT = radiation therapy.

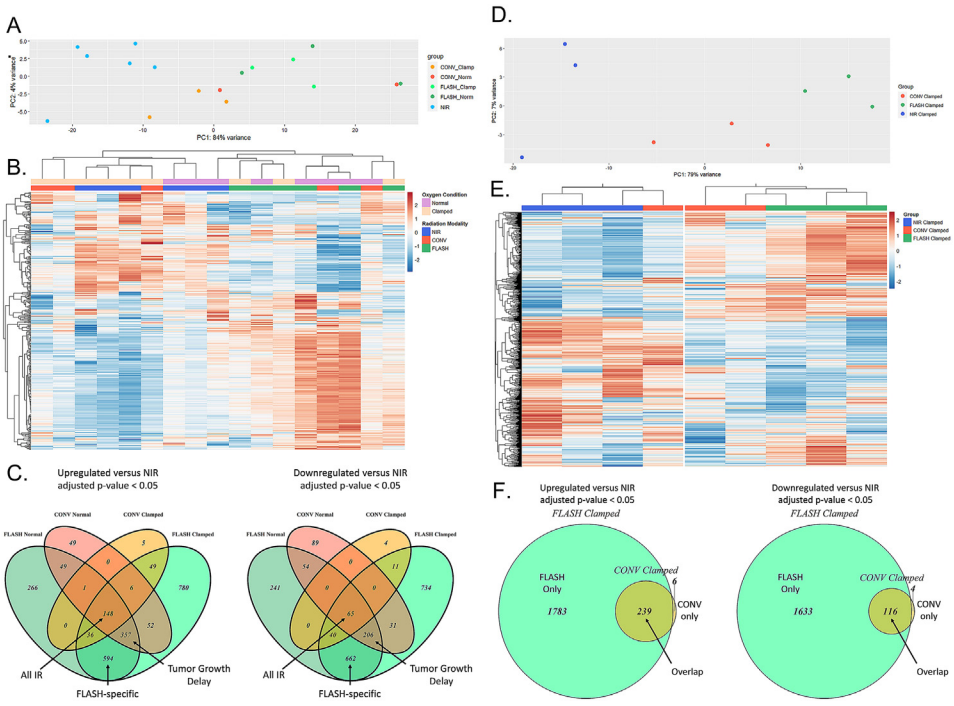

Fig. 2. Tumor growth delay and FLASH-specific clusters identified for normal and clamped comparisons and for clamped-only comparisons. (A) PCA to visualize sample-to-sample distances based on the top 2 principal components (PC1 and PC2) for the normal and clamped conditions. (B) Heatmap with the same samples showing the top 500 genes, with columns (samples) and rows (genes, Z-score) clustered hierarchically. (C) Venn diagrams depicting the overlap of genes significantly (adjusted $P < .05$ from DESeq2 output) upregulated or downregulated in treated groups versus nonirradiated (NIR) controls. (D) PCA to visualize sample-to-sample distances based on the top 2 principal components (PC1 and PC2) for only the clamped condition. (E) Heatmap with the clamped samples showing the top 500 genes, with columns (samples) and rows (genes, Z-score) clustered hierarchically. (F) Venn diagrams depicting the overlap of genes significantly (adjusted $P < .05$ from DESeq2 output) upregulated or downregulated in treated groups versus NIR controls. *Abbreviation:* PCA = principal components analysis.

Using the DESeq2 output, we made lists of all differentially expressed genes in irradiated groups versus the NIR control group and determined all overlaps. We identified 3 main overlap profiles: FLASH-specific, which included genes changed significantly versus NIR in both FLASH normal and FLASH clamped groups but not in neither of the CONV groups with 594 upregulated genes and 662 downregulated genes found; tumor growth delay, which included genes changed significantly in FLASH clamped, FLASH normal, and CONV normal groups versus NIR but not the CONV clamped group with 357 upregulated and 206 downregulated genes found; and All-IR, which included genes changed significantly in all irradiated groups versus nonirradiated control with 148 upregulated and 63 downregulated genes found (Fig. 2C).

Applying the same analysis exclusively for clamped conditions 24 hours post-RT, the PCA showed distinct clusters for CONV clamped, FLASH clamped, and NIR clamped groups (Fig. 2D), clearly confirmed by the heatmap (Fig. 2E). This analysis resulted in only 3 possible profiles: genes altered in FLASH or CONV samples only, and genes altered in both FLASH and CONV samples. Using the same overlap strategy, we found that the FLASH-only signature in the hypoxic condition was associated with 1783 genes uniquely upregulated and 1633 genes uniquely downregulated (Fig. 2F). Using all overlap groups (FLASH-specific, tumor growth delay, All IR, FLASH only, overlap, and CONV only) we performed an overrepresentation analysis (ORA) of multiple databases including Wikipathways, Kyoto Encyclopedia of Genes and Genomes (KEGG), and Gene Ontology. Based on a global survey of the enrichments, we selected 3 main altered clusters of enrichments: (1) cell cycle, (2) translation and ribosome, and (3) HIF1 signaling and metabolism.

FLASH is more efficient than CONV at inhibiting cell cycle

We performed ORA analyses of downregulated genes, which showed enrichment for cell cycle−related pathways for the Wikipathways and KEGG databases in normal and clamped conditions (Fig. E6A, B). Although we found an enrichment of cell cycle and DNA replication in the genes

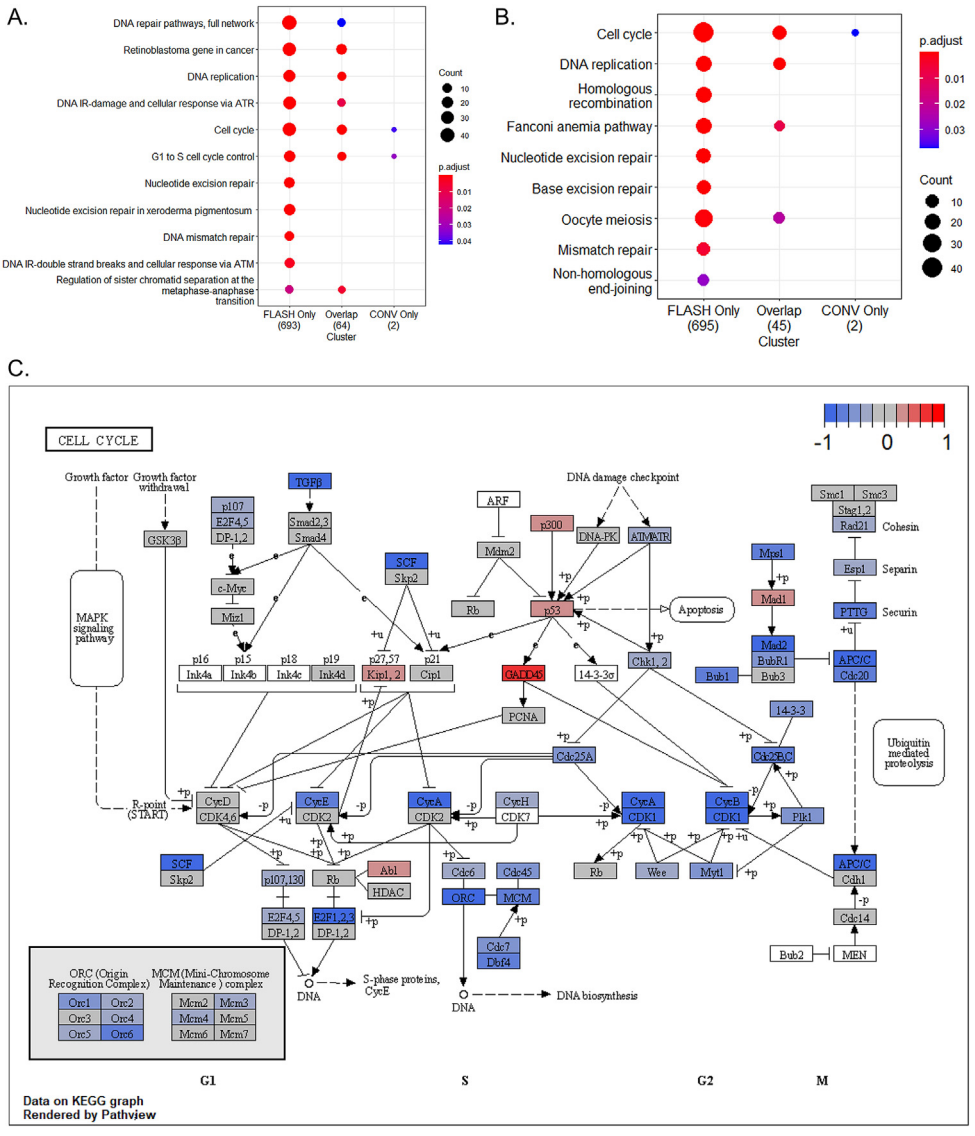

Fig. 3. Cell-cycle and DNA repair pathways further enriched in significantly downregulated genes in FLASH-treated group in clamped condition. (A) ORA for pathways from the Wikipathways database for DEG overlap clusters in clamped. (B) ORA for pathways from the KEGG database for DEG overlap clusters in clamped. (C) KEGG cell-cycle pathway with overlay of the log2 fold changes of FLASH versus CONV (clamped) from the DESeq2 output. *Abbreviations:* CONV = conventional dose rate; DEG = Differentially Expressed Gene; KEGG = Kyoto Encyclopedia of Genes and Genomes; ORA = overrepresentation analysis.

downregulated in the All-IR overlap, we detected further significant enrichments in the tumor growth delay overlap, and even more in the FLASH-specific overlap, suggesting an enhanced FLASH-induced inhibition of cell cycle–related pathways. Similarly, in analyzing the downregulated genes in only the clamped condition, we found enrichment for cell cycle–related pathways (Fig. 3A, B) in both FLASH only and Overlap groups and just minor enrichment in CONV only. This observation supports the trend of expanded downregulation of cell cycle–related genes by FLASH. By directly comparing the change in gene expression after FLASH and CONV in clamped and determining enrichments using gene set enrichment analysis (GSEA), we highlighted the downregulation of cell cycle–related genes as shown in Figure E6C and our GSEA plot (Fig. E6D). For the cell-cycle pathway (Fig. 3C), we observed a substantial downregulation (blue) in FLASH clamped versus CONV clamped, generally for the S (replication), G2 (growth and preparation for division), and M (mitosis) phases. Consistent with cell-cycle inhibition, we found that p53 effector *GADD45* was upregulated after FLASH clamped (middle, red), which could explain the inhibition of the cyclin B/CDK1 complex formation (of which both transcripts were found to be significantly downregulated).

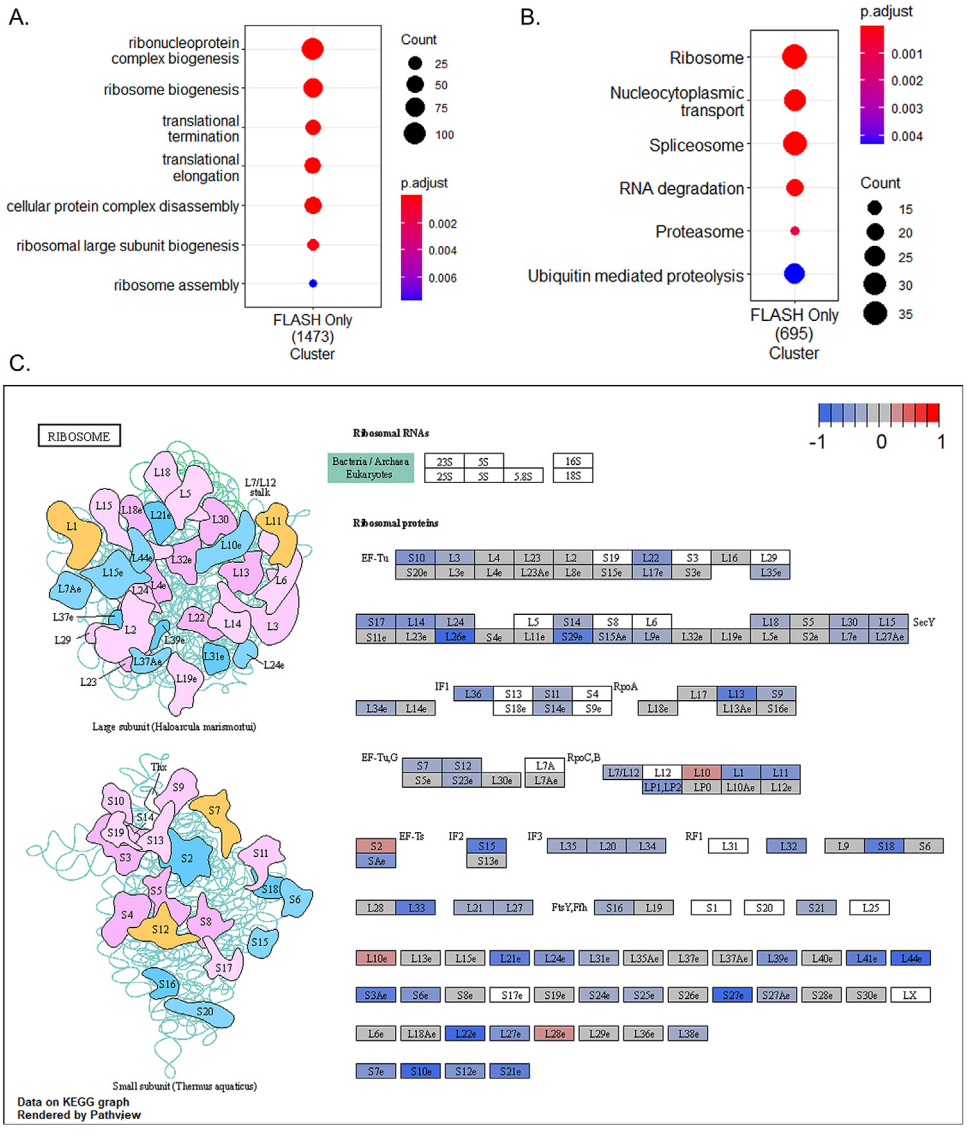

Fig. 4. Enrichment of ribosome biogenesis and translation unique to FLASH in clamped condition. (A) ORA for pathways from the GO database for DEG overlap clusters in clamped. (B) ORA for pathways from the KEGG database for DEG overlap clusters in clamped. (C) KEGG ribosome pathway with overlay of the log2 fold changes of FLASH versus CONV (clamped) from the DESeq2 output. *Abbreviations:* CONV = conventional dose rate; DEG = Differentially Expressed Gene; GO = Gene Ontology; KEGG = Kyoto Encyclopedia of Genes and Genomes; ORA = overrepresentation analysis.

Inhibition of translation and ribosomal biogenesis is FLASH-specific

Using the same ORA analyses of downregulated genes, we also identified enrichments for ribosome and translation for the Gene Ontology and KEGG databases in normal and clamped conditions (Fig. E7A, B). We found that these enrichments are largely specific to FLASH and not associated with the tumor growth delay or All IR overlaps. Similarly, in analyzing the downregulated genes in only the clamped condition, we found enrichment for ribosome- and translation-related pathways (Fig. 4A, B) exclusively in the FLASH only group.

Directly comparing the change in gene expression after FLASH and CONV in clamped condition and determining enrichments using GSEA, we highlighted downregulation of ribosome, mRNA processing, and protein turnover genes, as shown in Figure E7C and our GSEA plot (Fig. E7D). The representation of the ribosome pathway (Fig. 4C) showed widespread downregulation of ribosomal protein transcripts, for both large and small ribosomal subunits.

Discovery of a metabolic switch after FLASH exposure

Using ORA analysis of upregulated genes, we showed enrichment for HIF1 signaling and glycolysis for the Wikipathways and KEGG databases in normal and clamped

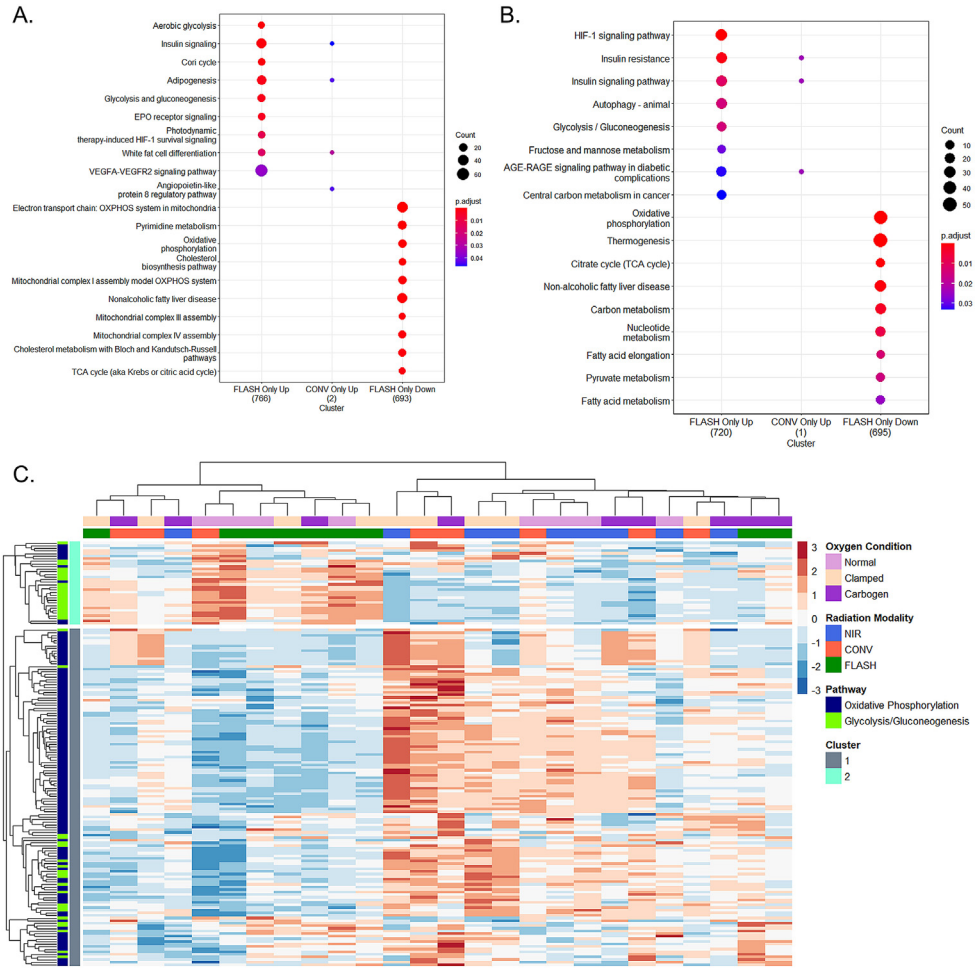

Fig. 5. Evidence of FLASH-specific metabolic switch. (A) ORA for pathways from the Wikipathways database for DEG overlap clusters in clamped. (B) ORA for pathways from the KEGG database for DEG overlap clusters in clamped. (C) Heatmap of exclusively glycolysis/gluconeogenesis and OXPHOS KEGG pathway genes for all oxygen conditions, with columns (samples) and rows (genes, Z-score) clustered hierarchically. *Abbreviations:* DEG = Differentially Expressed Gene; KEGG = Kyoto Encyclopedia of Genes and Genomes; ORA = overrepresentation analysis.

conditions (Fig. E8A, B). These enrichments were specific to the tumor growth delay overlap in other words occurred after CONV and FLASH irradiation except in the CONV clamped condition. The ORA analyses of downregulated genes also showed enrichment for oxidative phosphorylation (OXPHOS) that was exclusively FLASH-specific. In examining only the clamped condition, we found enrichment for HIF1 signaling (up), glycolysis/gluconeogenesis (up), and OXPHOS (down) only in the FLASH-only overlap (Fig. 5A, B). Comparing directly the change in gene expression after FLASH and CONV in clamped condition and determining enrichments using GSEA, we highlighted upregulation of hypoxia and glycolysis and downregulation of OXPHOS as shown in Figure E8C. Examination of the hypoxia and metabolic pathways (Fig. E8D-F) showed numerous upregulated targets downstream of HIF1A after FLASH clamped *versus* CONV Clamped (red, Fig. E9D), including targets related to anaerobic metabolism such as *GLUT1* (glucose transporter type 1), *HK2* (hexokinase 2), *ALDOA* (aldolase fructose-bisphosphate A), *ENO1* (enolase 1), *PGK1* (phosphoglycerate kinase 1), and *PFK2* (phophofructokinase 2). Specifically, we observed an upregulation of *PDK1* (pyruvate dehydrogenase kinase 1), which, in turn, causes inhibition of the tricarboxylic acid cycle and the electron transport chain, and stimulation of glycolysis. Therefore, our finding of upregulation of the main glycolytic pathway (red, Fig. E8E) in the FLASH-treated tumors compared with the CONV-treated tumors under vascular clamping was consistent with HIF activation. Interestingly, we also found that the section of the pathway responsible for converting pyruvate into acetyl-CoA for the tricarboxylic acid cycle was downregulated (blue), consistent with a lack of aerobic respiration. In addition, we observed the possibility of the oxaloacetate intermediate being shunted back into the glycolytic/gluconeogenic pathway. Moreover, our analysis revealed that the KEGG OXPHOS pathway (Fig. E8F) was downregulated in FLASH versus CONV samples across all 5 electron transport chain complexes, with multiple

components downregulated in each of the complex I-V, consistent with significant electron transport chain repression/disruption. To reinforce our ORA and GSEA data, we conducted an unsupervised clustering of all metabolic genes from these 2 pathways using a heatmap (Fig. 5C), which showed that the genes separated into 2 clusters—one mostly including OXPHOS genes and another composed mainly of glycolysis/gluconeogenesis genes. We found that the CONV-treated samples clustered mostly with the nonirradiated ones with greater expression in the OXPHOS cluster and lower expression in the glycolysis one. In contrast, the FLASH-treated samples from all oxygen conditions mostly clustered together with the OXPHOS cluster downregulated and the glycolysis cluster upregulated, suggesting that glycolysis may be a potential target to increase the antitumor efficacy of FLASH using this model.

Neoadjuvant treatment with trametinib

To target glycolysis after FLASH, we used a Food Drug Administration (FDA)-approved MEK 1/2/glycolysis inhibitor called trametinib as an adjuvant treatment. The treatment delayed the tumor relapse (Fig. 6A), improved survival (Fig. 6B; $P = .0079$), and significantly increased the mean doubling time of clamped tumors from 32.5 ± 0.9 days to 40.2 ± 1.6 days post-RT (Fig. 6C; $P = .0022$) and the mean doubling time of normal tumors from 35.3 ± 0.2 days to 43.8 ± 1.7 days post-RT ($P = .0034$). Although we observed improved tumor growth delay in both cases, our treatment regimen did not result in complete response. These findings suggest that we need to refine the administration schedule and/or investigate the involvement of other resistance mechanisms to enhance the treatment's efficacy.

Discussion

As the key finding of this study, we conclusively demonstrated the superior efficacy of FLASH against tumors placed under acute severe hypoxia compared with CONV. This result was not restricted to a single model, as we were able to reproduce and validate it in various human and murine tumor models implanted in immunodeficient and immunocompetent mouse strains. Our RNAseq results showed a direct imprint of the response to FLASH versus CONV at acute (24-hour) time-point post-RT, whereas at 1 week postrecurrence we found the imprint to be relapse-dependent rather than radiation response-dependent. Our in-depth analysis of the acute imprint revealed a FLASH-specific profile in clamped tumors that involved an arrest of cell cycle, mitosis, and ribosomal biogenesis, and a switch from OXPHOS to glycolysis. Moreover, inhibition of glycolysis with trametinib enhanced FLASH efficacy. Overall, this study highlights the efficacy of FLASH in radiation-resistant tumors, mediated by delayed growth and reduced

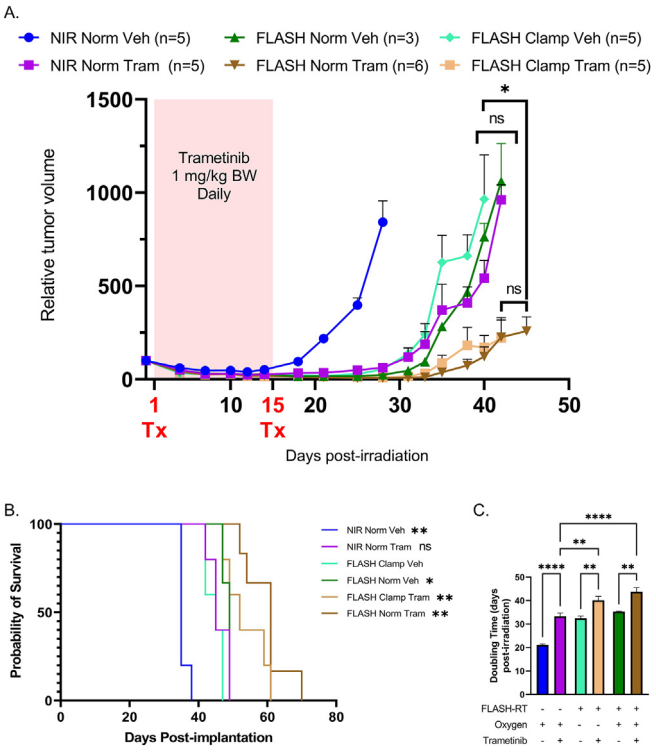

Fig. 6. Significant tumor growth delay via daily trametinib treatment for 14 days after FLASH. (A) Relative tumor volume of U-87 MG implanted subcutaneously in the flank of female nude mice treated with 20 Gy single fraction delivered with FLASH under normal and clamped conditions. Mean relative tumor volume ± SEM, N = 3 to 6 animals per group, as indicated. *P* values derived from endpoint analysis using a Kruskal-Wallis test with *post hoc* Dunn's correction for multiple testing: $^{*}P < .05$. (B) Kaplan-Meier survival curves for animals stratified by radiation modality, tumor oxygenation, and treatment group. *P* value derived from log rank (Mantel-Cox) test: $^{*}P < .05$; $^{**}P < .01$. (C) Doubling times calculated for each group. Mean days post-RT ± SEM, N = 3 to 5 animals per group, as indicated. *P* values derived from one-way ANOVA followed by *post hoc* Šídák correction for multiple testing: $^{**}P < .01$; $^{****}P < .0001$. *Abbreviations:* ANOVA = analysis of variance; CONV = conventional dose rate; ns = not significant; RT = radiation therapy.

proliferation, and provides a novel if not compelling rationale to use FLASH instead of CONV.

Radiation resistance is complex and involves combination of extrinsic signals from the microenvironment and intrinsic factors that characterize the tumors. In this study, we investigated one extrinsic signal, tumor hypoxia which represents one of the major root causes of cancer treatment resistance when RT at conventional dose rate is used but also impairs the therapeutic outcome of CT. The relationship between tumor oxygenation and the efficacy of RT is well-known and has been extensively characterized.[27] Our present data obtained with CONV directly reflected this

relationship. We found that tumors irradiated in carbogen conditions experienced a longer growth delay (+5 days doubling time vs normal conditions), whereas clamped tumors exhibited less favorable control (−8.6 days doubling time vs normal). Conversely, FLASH challenges this long-standing paradigm with no significant difference in doubling time and growth curves between normal and clamped tumors. Our results also suggest that the sensitivity of clamped tumors to FLASH is not restricted to a single and/or specific model but can be generalized and replicated across various human and murine tumor models. In addition, we observed a similar outcome in immunocompromised and competent hosts, which does not support a specific contribution of the (adaptive) immune system. We measured intratumoral oxygen tension directly and noninvasively using the Oxyphor PtG4 probe and OxyLED system[8,28-31] and we stained for hypoxia in situ using pimonidazole. We were able to confirm severe hypoxia (0-2 mm Hg O_2, <0.3% O_2) within minutes after clamping, whereas carbogen breathing resulted in an increase in tumor pO_2 consistent with the literature.[32,33] Although this acute hypoxia induces radioresistance to CONV, it is worth noting that this model is an acute, artificial hypoxia that cannot recapitulate prolonged and chronic hypoxia observed in many cancers. However, we found that FLASH offers superior control in this hypoxic condition, which is known to be treatment resistant.

Based on transcriptomic evidence, we suggest that increased tumor control and growth delay using the FLASH modality in clamped tumors was due to an inhibition of cell-cycle progression caused by specific downregulation of cell-cycle genes and proliferation pathways. For the clamped condition, we observed downregulation of several cell cycle −related genes in both dose-rate groups (Overlap). As a well-characterized response to ionizing radiation and DNA damage,[34] we expected it. However, we found an additional cluster of cell cycle−related genes was downregulated in the FLASH only list—with significant independent enrichments for cell cycle and DNA replication. From these data, we surmise that the differential tumor response between FLASH and CONV under clamped condition was related to a more complete versus partial cell-cycle arrest, respectively. Enhanced tumor growth delay observed under FLASH is likely dependent on elevated GADD45. Our observation of increased *GADD45* expression in the KEGG cell-cycle pathway analysis supports this idea. This result is consistent with a putative genomic imprint of FLASH susceptibility we shown previously in a patient-derived xenograft model of T-cell acute lymphoblastic leukemia.[10] The role of GADD45 in controlling activation of S and G2/M checkpoints after genotoxic stress by dissociating and inhibiting the kinase activity of the CDK1/CyclinB1 complex[35] suggests FLASH provides more robust control of proliferation.

We found that additional gene sets related to translation and ribosomal function were significantly downregulated in FLASH-treated groups in both normal and clamped conditions. The downregulation of ribosomal machinery is closely associated to cell-cycle arrest as previously shown in yeast, in which decreased ribosomal translation was sufficient to cause cell-cycle arrest in the G1 phase.[36] Moreover, translation inhibition by cycloheximide caused phosphorylation and activation of CHK1, which impaired G2/M cell-cycle progression.[37] The translation of cellular mRNAs to proteins by ribosomes can fuel the uncontrolled growth program of a tumor. In addition, the translation of mRNA into proteins has a high energy cost for cells,[38] which is why transient, radiation-induced inhibition of cap-dependent protein synthesis is a conserved cellular stress response.[39] Our results suggest that FLASH enhances the level of ribosomal stress in tumors, thus decreasing translation, which can induce further activation of cell-cycle checkpoints, thereby overriding the protective effects of hypoxia.

Next, we showed that the tumor growth delay outcome under acute hypoxia was associated with significant metabolic alterations 24 hours post-FLASH, and more specifically with an increased glycolysis and decreased OXPHOS gene expression. These changes are consistent with recently described alterations in cancer cell metabolism after *in vitro* exposure to ionizing radiation.[40] However, we did not detect such changes upon comparison of the CONV clamped group with the NIR clamped group, indicating that FLASH modulates the expression of these metabolic gene sets under acute hypoxia, whereas CONV does not. We also identified these changes in normally oxygenated normal tumors 24 hours posttreatment with FLASH, but only the decrease in OXPHOS gene expression was FLASH-specific. In other words, we found increased glycolysis gene expression in the CONV normal group as well, but not OXPHOS downregulation. It is important to note that release of the vascular clamp itself could lead to ROS-induced release of HIF1 target gene transcripts sequestered in stress granules,[41] but we performed this procedure in both modalities and in the NIR controls, so the confounding effect should be limited. We presented overwhelming evidence of these metabolic changes using ORA, GSEA, pathway analysis, and heatmap clustering of metabolic genes. In summary, we discovered a FLASH-specific metabolic switch in GBM 24 hours after irradiation.

The metabolic shift prompted us to use a glycolysis inhibitor, trametinib. Trametinib is an FDA-approved MEK1/2 inhibitor that can be administered orally and is well tolerated.[42] Results from a recent clinical trial provided evidence that that the drug could readily cross the blood-brain barrier in humans,[43] which is essential for GBM treatment. U-87 MG cells were previously shown to be sensitive to trametinib,[44] and this drug was found to inhibit growth (*in vitro* and *in vivo*) and aerobic glycolysis (*in vitro*) in other glioma models.[45] These features clearly boost the clinical relevance of our study, where we used trametinib as a short-term adjuvant treatment and showed its ability to enhance the antitumor efficacy of FLASH in the U-87 MG xenograft model under both normal and clamped conditions. This suggests that the combination of cell-cycle arrest and metabolic intervention are factors that are involved and can be exploited to optimize FLASH efficacy.

Conclusion

So far, the superiority of FLASH over CONV has largely been attributed to its capability to spare normal tissue from radiation-induced toxicities. In the present study, we bring the first evidence of an important additional benefit of FLASH, namely, efficacy against radioresistant hypoxic tumors. This sustained efficacy of FLASH in conditions known to promote radiation resistance suggests that FLASH targets an intrinsic (death) signal more potently than CONV. The signal remains to be formally identified but could be related to the regulation of the G2/M transition, and our findings showing that FLASH induces inhibition of proliferation and translation support this idea. Notably, we also uncovered a druggable metabolic switch that we successfully reversed using the FDA-approved compound trametinib to enhance the efficacy of FLASH. These mechanistic findings are fundamental and support the ultimate translation of FLASH into the clinic.

References

1. Vaupel P, Höckel M, Mayer A. Detection and characterization of tumor hypoxia using pO2 histography. *Antiox Redox Signal* 2007;9:1221-1236.
2. Zeng W, Liu P, Pan W, Singh SR, Wei Y. Hypoxia and hypoxia inducible factors in tumor metabolism. *Cancer Lett* 2015;356:263-267.
3. Graham K, Unger E. Overcoming tumor hypoxia as a barrier to radiotherapy, chemotherapy and immunotherapy in cancer treatment. *Int J Nanomedicine* 2018;13:6049-6058.
4. Vozenin M-C, Bourhis J, Durante M. Towards clinical translation of FLASH radiotherapy. *Nat Rev Clin Oncol* 2022;19:791-803.
5. Limoli CL, Vozenin M-C. Reinventing radiobiology in the light of FLASH radiotherapy. *Ann Rev Cancer Biol* 2023;7:1-21.
6. Vozenin M-C, Hendry JH, Limoli CL. Biological benefits of ultra-high dose rate flash radiotherapy: Sleeping beauty awoken. *Clin Oncol* 2019;31:407-415.
7. Favaudon V, Caplier L, Monceau V, et al. Ultrahigh dose-rate FLASH irradiation increases the differential response between normal and tumor tissue in mice. *Sci Transl Med* 2014;6:245ra93.
8. Cao X, Zhang R, Esipova TV, et al. Quantification of oxygen depletion during FLASH irradiation in vitro and in vivo. *Int J Radiat Oncol Biol Phys* 2021;111:240-248.
9. Fouillade C, Curras-Alonso S, Giuranno L, et al. FLASH irradiation spares lung progenitor cells and limits the incidence of radio-induced senescence. *Clin Cancer Res* 2020;26:1497-1506.
10. Chabi S, To THV, Leavitt R, et al. Ultra-high-dose-rate flash and conventional-dose-rate irradiation differentially affect human acute lymphoblastic leukemia and normal hematopoiesis. *Int J Radiat Oncol Biol Phys* 2021;109:819-829.
11. Ruan J-L, Lee C, Wouters S, et al. Irradiation at ultra-high (FLASH) dose rates reduces acute normal tissue toxicity in the mouse gastrointestinal system. *Int J Radiat Oncol Biol Phys* 2021;111:1250-1261.
12. Montay-Gruel P, Acharya MM, Gonçalves Jorge P, et al. Hypofractionated FLASH-RT as an effective treatment against glioblastoma that reduces neurocognitive side effects in mice. *Clin Cancer Res* 2021;27:775-784.
13. Jaccard M, Durán MT, Petersson K, Germond J-F, Liger P, Vozenin M-C, et al. High dose-per-pulse electron beam dosimetry: Commissioning of the Oriatron eRT6 prototype linear accelerator for preclinical use. *Med Phys* 2018;45:863-874.
14. Liao Y, Shi W. Read trimming is not required for mapping and quantification of RNA-seq reads at the gene level. *NAR Genom Bioinform* 2020;2:lqaa068.
15. Dobin A, Davis CA, Schlesinger F, et al. STAR: Ultrafast universal RNA-seq aligner. *Bioinformatics* 2013;29:15-21.
16. Li H, Handsaker B, Wysoker A, et al. The sequence alignment/map format and SAMtools. *Bioinformatics* 2009;25:2078-2079.
17. Kluin RJC, Kemper K, Kuilman T, et al. XenofilteR: Computational deconvolution of mouse and human reads in tumor xenograft sequence data. *BMC Bioinformatics* 2018;19:366.
18. R Core Team. R: A language and environment for statistical computing. Available at: https://www.R-project.org/. Accessed May 18, 2021.
19. RStudio Team. RStudio: Integrated development environment for R. Available at: http://www.rstudio.com/. Accessed May 24, 2021.
20. Liao Y, Smyth GK, Shi W. featureCounts: An efficient general purpose program for assigning sequence reads to genomic features. *Bioinformatics* 2014;30:923-930.
21. Love MI, Huber W, Anders S. Moderated estimation of fold change and dispersion for RNA-seq data with DESeq2. *Genome Biol* 2014;15:550.
22. Wu T, Hu E, Xu S, et al. clusterProfiler 4.0: A universal enrichment tool for interpreting omics data. *Innovation* 2021;2 100141.
23. Wickham H. ggplot2: Elegant graphics for data analysis. Available at: https://ggplot2.tidyverse.org. Accessed June 25, 2021.
24. Kolde R. pheatmap: Pretty heatmaps. Available at: https://cran.r-project.org/web/packages/pheatmap/index.html. Accessed June 28, 2021.
25. Luo W, Brouwer C. Pathview: An R/Bioconductor package for pathway-based data integration and visualization. *Bioinformatics* 2013;29:1830-1831.
26. Benjamini Y, Hochberg Y. Controlling the false discovery rate: A practical and powerful approach to multiple testing. *J Roy Stat Soc B (Methodol)* 1995;57:289-300.
27. Moulder JE, Rockwell S. Hypoxic fractions of solid tumors: Experimental techniques, methods of analysis, and a survey of existing data. *Int J Radiat Oncol Biol Phys* 1984;10:695-712.
28. Dunphy I, Vinogradov SA, Wilson DF. Oxyphor R2 and G2: Phosphors for measuring oxygen by oxygen-dependent quenching of phosphorescence. *Anal Biochem* 2002;310:191-198.
29. Esipova TV, Karagodov A, Miller J, Wilson DF, Busch TM, Vinogradov SA. Two new "protected" oxyphors for biological oximetry: Properties and application in tumor imaging. *Anal Chem* 2011;83:8756-8765.
30. Esipova TV, Barrett MJP, Erlebach E, et al. Oxyphor 2P: A high-performance probe for deep-tissue longitudinal oxygen imaging. *Cell Metab* 2019;29 736-744.e7.
31. El Khatib M, Van Slyke AL, Velalopoulou A, et al. Ultrafast tracking of oxygen dynamics during proton FLASH. *Int J Radiat Oncol Biol Phys* 2022;113:624-634.
32. Martin L, Lartigau E, Weeger P, et al. Changes in the oxygenation of head and neck tumors during carbogen breathing. *Radiother Oncol* 1993;27:123-130.
33. Falk SJ, Ward R, Bleehen NM. The influence of carbogen breathing on tumour tissue oxygenation in man evaluated by computerised p02 histography. *Br J Cancer* 1992;66:919-924.
34. Visconti R, Della Monica R, Grieco D. Cell cycle checkpoint in cancer: A therapeutically targetable double-edged sword. *J Exp Clin Cancer Res* 2016;35:153.
35. Vairapandi M, Balliet AG, Hoffman B, Liebermann DA. GADD45b and GADD45g are cdc2/cyclinB1 kinase inhibitors with a role in S and G2/M cell cycle checkpoints induced by genotoxic stress. *J Cell Physiol* 2002;192:327-338.
36. Shamsuzzaman M, Bommakanti A, Zapinsky A, Rahman N, Pascual C, Lindahl L. Analysis of cell cycle parameters during the transition from unhindered growth to ribosomal and translational stress conditions. *PLoS One* 2017;12 e0186494.
37. Thomas SE, Malzer E, Ordóñez A, et al. p53 and translation attenuation regulate distinct cell cycle checkpoints during endoplasmic reticulum (ER) stress*. *J Biol Chem* 2013;288:7606-7617.

38. Li G-W, Burkhardt D, Gross C, Weissman JS. Quantifying absolute protein synthesis rates reveals principles underlying allocation of cellular resources. *Cell* 2014;157:624-635.
39. Braunstein S, Badura ML, Xi Q, Formenti SC, Schneider RJ. Regulation of protein synthesis by ionizing radiation. molecular and cellular biology. *Am Soc Microbiol* 2009;29:5645-5656.
40. Krysztofiak A, Szymonowicz K, Hlouschek J, et al. Metabolism of cancer cells commonly responds to irradiation by a transient early mitochondrial shutdown. *iScience* 2021;24 103366.
41. Moeller BJ, Cao Y, Li CY, Dewhirst MW. Radiation activates HIF-1 to regulate vascular radiosensitivity in tumors: Role of reoxygenation, free radicals, and stress granules. *Cancer Cell* 2004;5:429-441.
42. Wright CJ, McCormack PL. Trametinib: First global approval. *Drugs* 2013;73:1245-1254.
43. Wen PY, Stein A, Bent M van den, et al. Dabrafenib plus trametinib in patients with BRAFV600E-mutant low-grade and high-grade glioma (ROAR): A multicentre, open-label, single-arm, phase 2, basket trial. *Lancet Oncol* 2022;23:53-64.
44. Kanemaru Y, Natsumeda M, Okada M, et al. Dramatic response of BRAF V600E-mutant epithelioid glioblastoma to combination therapy with BRAF and MEK inhibitor: Establishment and xenograft of a cell line to predict clinical efficacy. *Acta Neuropathol Commun* 2019;7:119.
45. Gao M, Yang J, Gong H, Lin Y, Liu J. Trametinib inhibits the growth and aerobic glycolysis of glioma cells by targeting the PKM2/c-Myc Axis. *Front Pharmacol* 2021;12.